PHYSICS AND TECHNOLOGY OF CRYSTALLINE OXIDE SEMICONDUCTOR CAAC-IGZO

FUNDAMENTALS

Edited by
Noboru Kimizuka and Shunpei Yamazaki

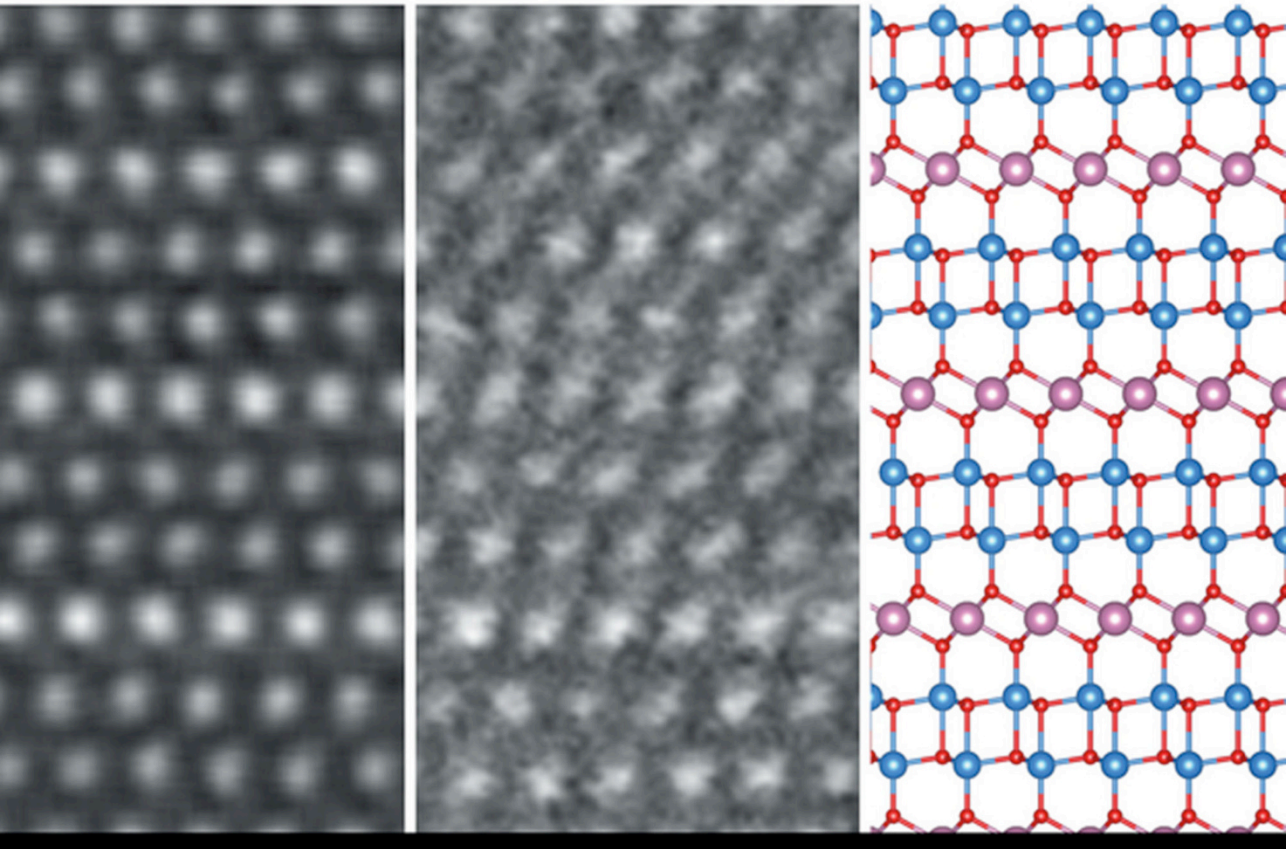

WILEY SID Series in Display Technology

PHYSICS AND TECHNOLOGY OF CRYSTALLINE OXIDE SEMICONDUCTOR CAAC-IGZO

Wiley-SID Series in Display Technology

Series Editors:
Anthony C. Lowe and Ian Sage

Display Systems: Design and Applications
Lindsay W. MacDonald and Anthony C. Lowe (Eds.)

Electronic Display Measurement: Concepts, Techniques, and Instrumentation
Peter A. Keller

Reflective Liquid Crystal Displays
Shin-Tson Wu and Deng-Ke Yang

Colour Engineering: Achieving Device Independent Colour
Phil Green and Lindsay MacDonald (Eds.)

Display Interfaces: Fundamentals and Standards
Robert L. Myers

Digital Image Display: Algorithms and Implementation
Gheorghe Berbecel

Flexible Flat Panel Displays
Gregory Crawford (Ed.)

Polarization Engineering for LCD Projection
Michael G. Robinson, Jianmin Chen, and Gary D. Sharp

Introduction to Microdisplays
David Armitage, Ian Underwood, and Shin-Tson Wu

Mobile Displays: Technology and Applications
Achintya K. Bhowmik, Zili Li, and Philip Bos (Eds.)

Photoalignment of Liquid Crystalline Materials: Physics and Applications
Vladimir G. Chigrinov, Vladimir M. Kozenkov, and Hoi-Sing Kwok

Projection Displays, Second Edition
Matthew S. Brennesholtz and Edward H. Stupp

Introduction to Flat Panel Displays
Jiun-Haw Lee, David N. Liu, and Shin-Tson Wu

LCD Backlights
Shunsuke Kobayashi, Shigeo Mikoshiba, and Sungkyoo Lim (Eds.)

Liquid Crystal Displays: Addressing Schemes and Electro-Optical Effects, Second Edition
Ernst Lueder

Transflective Liquid Crystal Displays
Zhibing Ge and Shin-Tson Wu

Liquid Crystal Displays: Fundamental Physics and Technology
Robert H. Chen

3D Displays
Ernst Lueder

OLED Display Fundamentals and Applications
Takatoshi Tsujimura

Illumination, Color and Imaging: Evaluation and Optimization of Visual Displays
Peter Bodrogi and Tran Quoc Khanh

Interactive Displays: Natural Human-Interface Technologies
Achintya K. Bhowmik (Ed.)

Addressing Techniques of Liquid Crystal Displays
Temkar N. Ruckmongathan

Fundamentals of Liquid Crystal Devices, Second Edition
Deng-Ke Yang and Shin-Tson Wu

Modeling and Optimization of LCD Optical Performance
Dmitry A. Yakovlev, Vladimir G. Chigrinov, and Hoi-Sing Kwok

PHYSICS AND TECHNOLOGY OF CRYSTALLINE OXIDE SEMICONDUCTOR CAAC-IGZO

FUNDAMENTALS

Edited by

Noboru Kimizuka
Kimizuka Institute for Natural Philosophy, Poland

Shunpei Yamazaki
Semiconductor Energy Laboratory Co., Ltd, Japan

WILEY

This edition first published 2017

Registered Office
John Wiley & Sons, Ltd, The Atrium, Southern Gate, Chichester, West Sussex, PO19 8SQ, United Kingdom

Library of Congress Cataloging-in-Publication Data

Names: Yamazaki, Shunpei, 1942– author. | Kimizuku, Noboru, 1940– author.
Title: Physics and technology of crystalline oxide semiconductor CAAC-IGZO.
Fundamentals / Shunpei Yamazaki, Noboru Kimizuku.
Other titles: Wiley SID series in display technology.
Description: Chichester, UK ; Hoboken, NJ : John Wiley & Sons, 2016. |
Series: Wiley-sid series in display technology | Includes index.
Identifiers: LCCN 2016022217 (print) | LCCN 2016033467 (ebook) | ISBN 9781119247401 (cloth) |
ISBN 9781119247364 (pdf) | ISBN 9781119247371 (epub)
Subjects: LCSH: Semiconductors–Materials. | Semiconductors–Characterization. | Gallium compounds. |
Zinc compounds.
Classification: LCC TK7871.85 .Y3576 2016 (print) | LCC TK7871.85 (ebook) | DDC 621.3815/2–dc23
LC record available at https://lccn.loc.gov/2016022217

A catalogue record for this book is available from the British Library.

Set in 10/12pt Times by SPi Global, Pondicherry, India

1 2017

Contents

About the Editors

Noboru Kimizuka is director of the Kimizuka Institute for Natural Philosophy in Poland and an adviser to Semiconductor Energy Laboratory Co., Ltd. He received a Doctor of Science degree from Tokyo Institute of Technology. He joined the National Institute for Research in Inorganic Materials (NIRIM) of the Science and Technology Agency in 1967 (this later became the National Institute for Materials Science). In 1985, he synthesized crystalline IGZO for the first time in the world at NIRIM. He then devoted himself to developing homologous IGZO for about the next ten years. After leaving NIRIM, he served as a researcher and visiting professor, teaching young people at universities in the USA, UK, Mexico, Taiwan, South Korea, and Japan. He is a member of the Chemical Society of Japan, the Ceramic Society of Japan, the Physical Society of Japan, and the American Ceramic Society. He is a resident of Poland.

1967	Completed Master's Degree Program at Waseda University Faculty of Science and Engineering
1967–1994	National Institute for Research in Inorganic Materials, Science and Technology Agency 1994–1995: Guest Researcher April 1983: Group Leader April 1975: Senior Researcher April 1967: Engineering Official of General Administrative Agency of the Cabinet
1969	Awarded by Joint Committee on Powder Diffraction Standards (JCPDS)
1969–1970	Foreign Researcher, Department of Materials Science, Pennsylvania State University (USA)
1977	Ceramographic Award of the Ceramic Society of Japan
1979–1980	Foreign Researcher, Department of Chemical Engineering, University of Texas at Austin (USA)
1993–1994	Instructor, Interdisciplinary Graduate School of Science and Engineering of Tokyo Institute of Technology
1994	Foreign Researcher, Department of Chemistry, University of Aberdeen (UK)

1994	Award by the Minister of the Science and Technology Agency of Japan
1994–1996	Dispatched Long-Term Expert, Japan International Cooperation Agency (JICA)
1994–2001	Research Professor, Universidad de Sonora (Mexico)
2001–2003	Visiting Scholar, Ceramic Material Research Institute, Hanyang University (South Korea)
2003–2005	Guest Researcher, National Institute for Materials Science (NIMS)
2006	Guest Professor, Department of Chemical Engineering & Material Science, Yuan Ze University (Taiwan)
2009–2010	Guest Professor, Department of Physics, Faculty of Science, Okayama University
2013	Guest Professor, Universidad de Sonora (Mexico)

Shunpei Yamazaki received his Ph.D., ME, BE, and honorary degrees from Doshisha University, Japan, in 1971, 1967, 1965, and 2011, respectively, and is the founder and president of Semiconductor Energy Laboratory Co., Ltd. He invented a basic device structure of non-volatile memory known as "flash memory" in 1970 during his Ph.D. program. Yamazaki is a distinguished foreign member of the Royal Swedish Academy of Engineering Sciences and a founder of Kato & Yamazaki Educational Foundation. Yamazaki has published or co-published over 400 papers and conference presentations and is the inventor or co-inventor of over 6314 patents (Guinness World Record in 2011).

1967	Completed Master's Degree Program at Doshisha University Graduate School of Engineering
1970	Invented a basic device of flash memory (Japanese Patent No. 886343; Japanese Examined Patent Application Publication No. Sho50-36955)
1971	Received Ph.D. in Engineering from Doshisha University Graduate School Doctoral Program Joined TDK Corporation (formerly TDK Electronics Co., Ltd.)
1980	Established Semiconductor Energy Laboratory Co., Ltd. and assumed position as president
1984	Awarded the Richard M. Fulrath Award by the American Ceramic Society (for research on MIS structure)
1995	Awarded the Medal with Dark Blue Ribbon from the Cabinet Office of the Japanese government (proceeds given to Japanese Red Cross Society) (awarded 6 times since 2015)
1997	Awarded the Medal with Purple Ribbon from the Cabinet Office of the Japanese government (for development of MOS LSI element technology)
2009	IVA (Royal Swedish Academy of Engineering Science) Foreign Member
2010	Awarded Okochi Memorial Technology Award from Okochi Memorial Foundation
2011	IEEE Life Fellow Received Honorary Doctor Degree of Culture from Doshisha University Renewed his first Guinness World Record in 2004 (man holding the most patents in the world)
2015	Granted the title of "Friend of Doshisha" by Doshisha University
2015	SID Special Recognition Award for "discovering CAAC-IGZO semiconductors, leading their practical application, and paving the way to next-generation displays by developing new information-display devices such as foldable or 8 K × 4 K displays"

List of Contributors

Noboru Kimizuka (editor)	Kimizuka Institute for Natural Philosophy
Shunpei Yamazaki (editor)	Semiconductor Energy Laboratory Co., Ltd.

In alphabetical order:

Koji Dairiki	Semiconductor Energy Laboratory Co., Ltd.
Tomoki Hiramatsu	Semiconductor Energy Laboratory Co., Ltd.
Ryunosuke Honda	Semiconductor Energy Laboratory Co., Ltd.
Noritaka Ishihara	Semiconductor Energy Laboratory Co., Ltd.
Erumu Kikuchi	Semiconductor Energy Laboratory Co., Ltd.
Yoshiyuki Kurokawa	Semiconductor Energy Laboratory Co., Ltd.
Yoichi Kurosawa	Semiconductor Energy Laboratory Co., Ltd.
Shinpei Matsuda	Semiconductor Energy Laboratory Co., Ltd.
Hiroyuki Miyake	Semiconductor Energy Laboratory Co., Ltd.
Motoki Nakashima	Semiconductor Energy Laboratory Co., Ltd.
Yusuke Nonaka	Semiconductor Energy Laboratory Co., Ltd.
Masashi Oota	Semiconductor Energy Laboratory Co., Ltd.
Takashi Shingu	Semiconductor Energy Laboratory Co., Ltd.
Nao Sorida	Semiconductor Energy Laboratory Co., Ltd.
Masahiro Takahashi	Semiconductor Energy Laboratory Co., Ltd.
Masashi Tsubuku	Semiconductor Energy Laboratory Co., Ltd.
Kazuhiro Tsutsui	Semiconductor Energy Laboratory Co., Ltd.
Yoshinori Yamada	Semiconductor Energy Laboratory Co., Ltd.
Michiko Yano	Semiconductor Energy Laboratory Co., Ltd.

Series Editor's Foreword

The introduction of active matrix backplanes into mainstream display technologies has arguably been more significant for the development of man–machine interaction than any one of the electro-optic effects which are exploited. Universally, the large and high-quality displays we use every day rely on active matrix switching, with only the smallest and simplest devices using passive addressing.

A variety of semiconductor materials and devices have been explored for this purpose: the performance advantages of compound semiconductors (such as cadmium selenide) have been well rehearsed, and polycrystalline silicon as well as single-crystal silicon have long been exploited for high-resolution applications. However, since the 1980s, hydrogenated amorphous silicon (a-Si:H) has become established as the commodity route to high-quality liquid crystal displays and has been overwhelmingly the dominant approach to their manufacture. Now this dominance is challenged, on the one hand by the promise of reduced manufacturing costs through the use of low-temperature and solution-processed materials and on the other hand with the drive towards higher pixel counts and resolution, as well as the introduction of active matrix OLED displays, having prompted a re-examination of crystallised forms of silicon and of amorphous and crystalline oxide-based semiconductors.

The present volume is the first in a series of three books which are planned to provide a comprehensive account of one approach to oxide semiconductor technology – the *c*-axis-aligned crystal (CAAC) morphology. The CAAC approach provides TFTs with high mobility and extremely low leakage current, and moreover avoids the stability problems found in some other oxide devices. Dr. Yamazaki and his co-authors bring to this topic not only their outstanding knowledge and research background, but also a real passion for explaining the properties and applications of the materials and devices they describe.

This book takes the reader from the deposition equipment and conditions needed to obtain CAAC oxide materials, through accounts of their structure and properties, to the properties and advantages of CAAC TFTs. A full account of the structural characterisation of the materials is included, together with their interpretation, as well as descriptions of the special measurement methods needed to understand these materials and the performance of CAAC TFTs, together

with a comparison with silicon devices. A brief account of the applications of CAAC oxide semiconductors concludes the volume.

Further series volumes will provide detailed accounts of the application of CAAC oxides to LSI (including imaging sensor) applications, and to displays. The value of CAAC oxide systems has already been demonstrated by the production of a number of exceptional high-resolution and high-complexity displays. As this exciting field develops, we expect that these books will provide the reader with a definitive source work and technical reference.

Ian Sage
Malvern, UK, 2016

Preface

Entering the 21st century, it seems that the growth of the electronics industry is hitting saturation level, even though it is the largest industry in the world. This is because the amount of energy used by people, which has already become enormous – as reflected in the abrupt climate change in recent years – is going to increase even more with its growth. Especially, the energy consumptions of cloud computing and electronic devices such as smartphones and supercomputers will continue to increase. Therefore, it is not an exaggeration to say that the development of new energy-saving devices has a direct influence on the continued existence of all mankind.

For this reason, we started extensive research on crystalline oxide semiconductors (OS), especially on a *c*-axis-aligned crystalline indium–gallium–zinc oxide (CAAC-IGZO) semiconductor. Due to the economic downturn in the aftermath of the Lehman Brothers' bankruptcy in the autumn of 2008, many companies withdrew from research on this subject, but I never gave up and our research in this area has continued to the present day. One of the most important characteristics of a field-effect transistor (FET) using this wide-gap semiconductor is that the off-state current is on the order of yoctoampère per centimeter (10^{-24} A/cm) (yocto is the smallest SI prefix), which is smaller than that of any other device measured so far. This characteristic effectively reduces the energy consumption, and thus we believe that it coincides with society's need to save energy.

It has been less than 10 years since I started researching and developing oxide semiconductors, but I think that proposing their effectiveness without delay is the first step toward a contribution to humanity. That is why I would like to introduce this book series, *Physics and Technology of Crystalline Oxide Semiconductor*, consisting of *Fundamentals*, *Application to LSI*, and *Application to Displays*, even though I know that it cannot be said that every detail is completely covered in the book series.

The book series contains the discovery of CAAC-IGZO by me, Shunpei Yamazaki, one of the editors and authors thereof, as well as the research results on its application obtained at Semiconductor Energy Laboratory Co., Ltd. (SEL), where I serve as president. We have decided to write the experimental facts down in as much detail as possible, and publish models whose principles have yet been verified. The reason is that I would like to give a couple of hints to readers – graduate students, on-site researchers, and developers – so that they can conduct

further R&D as soon as possible. For these reasons, as well as the limited number of pages, I would like you to accept my deepest apologies for not being able to publish all of the data in these books. Even after the publication of these three books about crystalline oxide semiconductors, I would like to continue making our CAAC-IGZO technology known to the public by conducting further research on it from both engineering and academic points of view.

This book covers a wide range of topics such as an In_2O_3–Ga_2O_3–ZnO-based material, related compounds thereof, and devices (displays and LSI) using a CAAC-IGZO. Regarding this book, for those who want to know more about the IGZO crystal, please start reading from Chapter 1. If you would like to know how to make CAAC-IGZO films, please turn to Chapter 2. For all those among you who would like to know more about the physical properties of IGZO, please begin with Chapter 3. If you would like to know CAAC-IGZO's applications, please start from Chapter 4.

In the past, Bell Laboratories published a set of books called *The Bell Telephone Laboratories series* about the invention of transistors and research results thereof, which accordingly spread the current concept of transistors throughout the world. We sincerely hope that our book series will help to spread the CAAC-IGZO technology just as *The Bell Telephone Laboratories series* helped to popularize the concept of transistors. I think that CAAC-OS, especially CAAC-IGZO, still has many unexplored possibilities and thus more institutions and scientists should research it in cooperation with each other. I am expecting that the CAAC-IGZO which we discovered will flourish in the 21st century, by publishing its physical properties and principles, as well as by applying it in the display and LSI fields, especially in energy-saving devices.

So far, we have made some efforts by submitting papers and giving presentations at various conferences about crystalline oxide semiconductors and OS FETs. However, we have never heard of another case where a ceramic was used for an active element on a mass-production basis in Si LSI or displays; thus, many companies (with the exception of Sharp Corporation) will face a lot of difficulties in terms of mass production. Note that a ceramic with an amorphous structure has been proposed before, but it was not put into practical use due to reliability problems. Especially, the great depression following 2008 made many companies quit their R&D of ceramics with an amorphous structure, which was deemed to be fruitless because a FET utilizing amorphous ceramic lacks reliability. The actual reasons are that many oxygen vacancies (V_O) as well as hydrogenated oxygen vacancies generated by hydrogen trapped in V_O exist in a less-crystallized IGZO. This book also covers that point.

I, Shunpei Yamazaki, observed a TEM image of an IGZO film in front of a TEM screen to find a solution for this reliability issue. At that time, I discovered that a CAAC structure existed in the IGZO film. I thought that the problem of reliability could be solved by the use of this kind of material, and thus shifted the focus of our R&D to CAAC-IGZO. A FET using this CAAC-IGZO has a high level of reliability, which cannot be said about FETs which use amorphous IGZO. Thus, a FET with CAAC-IGZO is excellent from a repeatability point of view in that it can be measured and evaluated stably, both on the material and device level. As a result of the stable measurement and evaluation, we discovered that the off-state current is on the order of yoctoamps per centimeter (10^{-24} A/cm), as mentioned above. Additionally, since IGZO has a wide solid-solution phase, we succeeded in fabricating FETs using CAAC-IGZOs having high mobilities of 30–70 cm^2/V-s, thus exceeding 50 cm^2/V-s, by changing the composition ratio and the device structure. A mobility equaling that of an LTPS-FET means that the CAAC-IGZO might not only be able to fight evenly with an LTPS-FET, but outperform it in the industry. Furthermore, we tried to apply CAAC-IGZO FETs to LSI, something which has

never been done before, and discovered that such a FET can operate with a channel length of just 20–60 nm.

Our data has been reviewed by many specialists, but it seems that to help people understand *the true value of the crystalline oxide semiconductor*, there is still a need to further explain the numerous issues concerning fundamental properties, which have not yet been fully understood. Moreover, a lot of people gave us the same advice: to help intellectuals grasp the whole picture of the technology by publishing a series of at least three books (*Fundamentals*, *Application to LSI*, and *Application to Displays*). Accordingly, I decided to publish them. Note that almost the whole content of these books is based on our experimental data. Hence, please acknowledge SEL and Advanced Film Device Inc. (AFD Inc.), a subsidiary of SEL, as the sources of these books, unless otherwise specified.

During the creation of this book, many people helped and guided us. I would like to express my sincere appreciation especially to Dr. Noboru Kimizuka, who was the first scientist in the world to have succeeded in the synthesis of IGZO. He has given us his guidance as a corporate adviser over the past several years, and kindly accepted our offer to become an editor and co-author of *Fundamentals*.

Moreover, during the research and development on which these books are based, as well as during the writing process, many young researchers at SEL also contributed. The names of all the authors involved can be found in the List of Contributors.

We would also like to extend our heartfelt thanks to Dr. Johan Bergquist, Dr. Michio Tajima, Dr. Yoshio Waseda, and Mr. Jun Koyama for helping us with the English translation of this book – by checking for errors and giving us a great deal of advice on how to improve the text.

I was blessed with support and cooperation from many outstanding individuals. I would like to add that I could not have finished these books in such a short period of time without the efforts of Dr. Ian Sage, a Wiley-SID book series editor, who suggested the publication of the books within this time, as well as Ms. Alexandra Jackson and Ms. Nithya Sechin of John Wiley & Sons, Ltd. Last but not least, I would like to express my sincere gratitude to those publishers and authors who allowed us to use their figures as references in these books.

Shunpei Yamazaki
President of Semiconductor Energy Laboratory Co., Ltd.

Acknowledgments

First of all, we would like to thank **Dr. Johan Bergquist**, **Dr. Michio Tajima**, **Dr. Yoshio Waseda**, and **Mr. Jun Koyama**, who encouraged us and gave us valuable advice on writing manuscripts.

Furthermore, we would also like to thank many people in a variety of fields for providing data, cooperation in manuscript writing and English translation, and all other aspects of this book.

Our heartfelt thanks to (in alphabetical order)

Ms. Mayumi Adachi
Mr. Shunsuke Adachi
Mr. Kengo Akimoto
Ms. Yukari Amano
Mr. Tobias Breitling
Ms. Nana Fujii
Mr. Shuji Fukai
Mr. Takafumi Fukumoto
Mr. Kazuma Furutani
Mr. Hiromichi Godo
Ms. Ai Hattori
Mr. Masahiko Hayakawa
Mr. Takuya Hirohashi
Mr. Takashi Igarashi
Ms. Yasuko Iharakumi
Mr. Takayuki Inoue
Mr. Shunichi Ito
Mr. Hiroshi Kanemura
Dr. Kiyoshi Kato
Mr. Hideyuki Kishida
Mr. Yoshiyuki Kobayashi
Mr. Junichi Koezuka
Ms. Yuko Konno
Mr. Keiichi Kurita
Ms. Michiyo Mashiyama
Dr. Daisuke Matsubayashi
Dr. Masakazu Murakami
Mr. Tsutomu Murakawa
Ms. Tomoko Nakagawa
Mr. Hasumi Nomaguchi
Mr. Satoru Okamoto
Mr. Kenichi Okazaki
Ms. Yoko Otake
Ms. Yu Sasaki
Mr. Yusuke Sekine
Mr. Akihisa Shimomura
Ms. Tamae Takano
Ms. Takako Takasu
Ms. Mika Tatsumi
Ms. Hitomi Tsurui
Mr. Ryosuke Watanabe
Mr. Yuto Yakubo
Mr. Ryo Yamauchi
Ms. Chiaki Yamura
and many others…

Noboru Kimizuka
Shunpei Yamazaki

Introduction

Physics and Technology of Crystalline Oxide Semiconductor CAAC-IGZO is composed of three books: *Fundamentals*, *Application to LSI*, and *Application to Displays*. Their association is shown in Figure 1.

This book, *Fundamentals*, presents characteristics of materials for an oxide semiconductor and its film-deposition mechanism. Specifically, this book covers results of atomic-level crystal structure analysis in nanometer order using high-resolution transmission electron microscopy (TEM) images, and proposes the deposition mechanism of *c*-axis-aligned crystalline indium–gallium–zinc oxide (CAAC-IGZO). Moreover, besides the fundamental properties of CAAC-IGZO, the electrical characteristics of CAAC-IGZO field-effect transistors (FETs) and a comparison of CAAC-IGZO FETs and silicon (Si) FETs are shown.

In *Physics and Technology of Crystalline Oxide Semiconductor CAAC-IGZO*, *Fundamentals* is positioned as the trunk, branching into *Application to LSI* and *Application to Displays*.

Application to LSI is expressed by one thick branch extending toward the miniaturization and integration (hybrid process) of LSI devices. It describes the process technologies of CAAC-IGZO FETs: a microfabrication process, a combination with Si process, and a combination process with other components such as wirings, insulating films, and capacitors. As fruits of these technologies, memories, CPUs, image sensors, and integrated circuits such as field-programmable gate arrays (FPGAs) are introduced.

Application to Displays is another thick branch extending toward high productivity and large-sized display devices. It describes the process technologies of CAAC-IGZO transistors: manufacturing process flows for a variety of types of transistor, a large-sized substrate, high productivity, low cost, and a combination with other components such as wirings, insulating films, and capacitors. The book covers, for application to organic light-emitting diode (OLED) displays and liquid crystal displays (LCDs) using CAAC-IGZO thin-film transistors (TFTs), TFT characteristics, driver circuits for display devices, high-resolution technology, low-power-consumption technology, transfer technology, and so on. As fruits of these technologies, a variety of prototyped displays (e.g., OLED displays, LCDs, and flexible displays) are introduced. In particular, the off-state current characteristic, which is the most outstanding feature, is explained in detail.

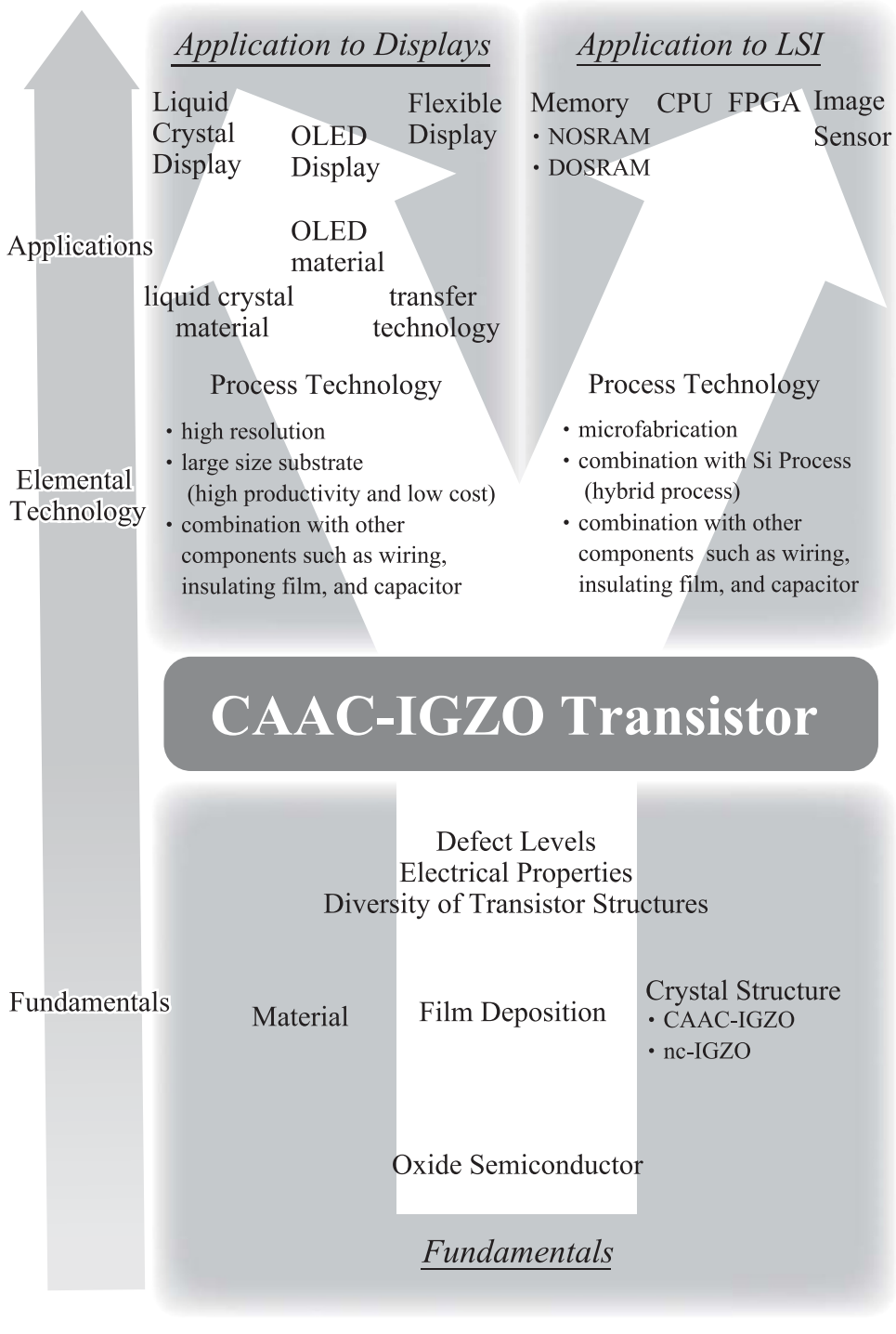

Figure 1 Framework of *Physics and Technology of Crystalline Oxide Semiconductor CAAC-IGZO*

The three books are closely associated with each other. Besides *Fundamentals*, *Application to LSI* and *Application to Displays* are of value to readers who might be interested in the basic theories and fabrication process of CAAC-IGZO devices. Data and references in these two books will also be useful to readers. The editors hope that this book series will be a foundation for the further development of CAAC-IGZO technology.

1

Layered Compounds in the In_2O_3–Ga_2O_3–ZnO System and Related Compounds in the Ternary System

1.1 Introduction

Indium–gallium–zinc oxide (IGZO) has gained traction as a novel semiconductor material in electronics. IGZO thin-film transistors are currently employed in the backplanes of mass-produced flat-panel displays, and their potential in various devices has been discussed in recent studies. The features and physical properties of IGZO differ from those of silicon, which is widely used in electronic devices. For instance, IGZO is a multi-component oxide with three cations. Furthermore, the distinctive layered structure of IGZO has led to the discovery of a new crystal morphology, *c*-axis-aligned crystalline IGZO (CAAC-IGZO), which will be detailed in the following chapters. The present chapter mainly describes the phase equilibrium diagrams of multi-component oxides and crystal structures of $InGaO_3(ZnO)_m$ ($m > 0$) with layered structures.

The properties of IGZO vary with the composition ratio of the metal elements. The bandgaps of In_2O_3, ZnO, and Ga_2O_3 (with different chemical compositions) are 2.6–2.9 [1, 2], 3.4 [3], and 4.8 eV [4], respectively. IGZO exhibits semiconductor properties in a relatively wide range of the phase equilibrium diagram. In the ZnO–$InGaZnO_4$ system, because ZnO and $InGaO_3(ZnO)$ ($m = 1$) show semiconductor properties, we speculate that a series of $InGaO_3(ZnO)_m$ will also behave as semiconductors. The $InGaO_3(ZnO)_m$ series has a layered structure in which O^{2-} is two-dimensional close-packed but may not be in contact with each other. This structure is closely related to the crystal morphology of CAAC-IGZO films, which will be described in the next chapter.

Physics and Technology of Crystalline Oxide Semiconductor CAAC-IGZO: Fundamentals, First Edition.
Edited by Noboru Kimizuka and Shunpei Yamazaki.

From the 1950s through the 1960s, the National Bureau of Standards [NBS, currently the National Institute of Standards and Technology (NIST)] in the United States comprehensively investigated the phase relationships of binary oxide systems such as R_2O_3–R'_2O_3, R_2O_3–A_2O_3, and R_2O_3–TiO_2 at temperatures up to 1800°C under atmospheric pressure. Here, R and R' denote lanthanides, Y, or Sc; A denotes Fe, Ga, Cr, or Al. Consequently, the NBS reported the thermochemical stability and crystal structures of the cationic elements in RAO_3 (perovskite), $R_3A_5O_{12}$ (garnet), magnetoplumbite, and $R_2Ti_2O_7$ (pyrochlore) [5–7]. Independently of the NBS research, Kimizuka and coworkers [8–17] added oxides of divalent cations, BO, to the binary system and investigated the resulting ternary system. This investigation, performed in the 1970s, is historically important as an extension of the NBS studies to a ternary system. In their systematic search for materials, Kimizuka and colleagues experimentally determined the phase equilibrium diagrams of the R_2O_3–A_2O_3–BO system at high temperatures and found a large number of $(RAO_3)_nBO$ and $RAO_3(BO)_m$. Here, R is a lanthanide, Y, In, or Sc; A is a trivalent cation and B is a divalent cation; m and n are natural numbers with no identified upper limits.

Subsequently, some $RAO_3(BO)_m$-type and $(RAO_3)_nBO$-type single crystals were grown, and their structures determined using single-crystal X-ray diffraction analysis. In addition, sintered powder bodies of these compounds were analyzed by powder X-ray diffraction and by electron beam diffraction. Consequently, the crystal structure of the homologous compounds $RAO_3(BO)_m$ was revealed: the R cation is located within the octahedral coordination of the O^{2-} anions, and the A and B cations are located within the trigonal-bipyramidal and tetrahedral coordination of the O^{2-} anions. All cations and anions in these oxides lie on the triangular lattice, and the O^{2-} anions stack perpendicular to the c-axis of the hexagonal crystal system [18–23]. The basic crystal structure was determined by analyzing $YbFe_2O_4$, an $RAO_3(BO)_m$ member with $m = 1$ [18]. The crystal structures of AB_2X_4-type compounds, classified by their coordination numbers, are listed in Table 1.1 [8, 24]. In the $YbFe_2O_4$-type crystal structure, R^{3+} occupies the sites of 6-fold oxygen octahedral coordination, and the A^{3+} and B^{2+} cations locate in the 5-fold oxygen trigonal-bipyramidal coordination. The $InGaO_3(ZnO)_m$ group $InGaO_3(ZnO)$ is isostructural with $YbFe_2O_4$. Before the discovery of $YbFe_2O_4$, no AB_2X_4-type compounds with 5- and 6-fold coordination were known. Compounds with layered structures related to $RAO_3(BO)_m$, including aluminum carbonitrides [25, 26] and sulfides (containing indium, gallium, and zinc), have also been reported [27].

Table 1.1 Classification of crystal structures with the general formula AB_2X_4, based on the coordination number (CN) of their cations. *Source*: Reprinted from [8], Copyright (1985), with permission from Elsevier

	CN of B				
CN of A	4	5	6	8	9 and/or 10
4	Phenacite		Olivine, spinel	K_2WO_4	β-K_2SO_4
6		$YbFe_2O_4$	Sr_2PbO_4, Ca_2IrO_4, etc.		K_2NiF_4
8			$CaFe_2O_4$, $CaTi_2O_4$		

As noted above, the R_2O_3–A_2O_3–BO system includes $RAO_3(BO)_m$ compounds with layered structures. In particular, layered $InGaO_3(ZnO)_m$ can be synthesized over a wide compositional range, and each $InGaO_3(ZnO)_m$ has substitutional solid solutions in the range $In_{1+x}Ga_{1-x}O_3(ZnO)_m (-1 < x \leq 1)$. Although structural uniformity is difficult to achieve in a multi-component system, such wide-ranging composition and solid solution suppresses the structural variation among the various chemical compositions. Therefore, the fundamental properties of layered crystals in the In_2O_3–Ga_2O_3–ZnO system, which are not expected to vary significantly, are suitable for the mass production of semiconductor devices. Kimizuka's elucidation of the phase equilibrium in In_2O_3–Ga_2O_3–ZnO has contributed significantly to the subsequent technology and mass production of CAAC-IGZO devices.

As a prelude to the succeeding chapters, this chapter introduces the crystal structures and phase equilibrium diagrams at high temperatures in the R_2O_3–A_2O_3–BO system, including the layered oxides mentioned above. Section 1.2 describes the phase equilibrium diagrams of ternary systems, including $InGaO_3(ZnO)_m$, and shows that their characteristics are not limited to the In_2O_3–Ga_2O_3–ZnO system. Section 1.3 presents the crystal structure of $InGaO_3(ZnO)_m$ and its layer-stacking sequences, obtained in a crystal structure analysis of powdered and single-crystal specimens. Section 1.4 presents transmission electron microscopy (TEM) images of $InGaO_3(ZnO)_m$ (where m is non-integer) with a long-period disordered stacking sequence along an axis perpendicular to the layer. The methods used to acquire the scanning TEM (STEM) images [annular bright field (ABF) and high-angle annular dark field (HAADF)] are outlined in Appendix 1.A.

1.2 Syntheses and Phase Equilibrium Diagrams

Here we describe what led to the discovery of $InGaZnO_4$. The first important study was on a phase equilibrium diagram of the Y_2O_3–Fe_2O_3–FeO system at high temperatures [19, 28]. This system includes YFe_2O_4, a mixed-valence compound containing Fe^{2+} and Fe^{3+} which is isostructural with $InGaZnO_4$. Subsequently, the phase equilibrium diagram of the R_2O_3–Fe_2O_3–FeO system (R = Ho, Er, Tm, Yb, and Lu) was determined [29–32], and a new phase $(RFeO_3)_nFeO$ ($n > 0$) with members $(RFeO_3)$ FeO, $(RFeO_3)_2$ FeO, … was found. $RFeO_3$(FeO) and $(RFeO_3)_2$(FeO)are isostructural with $InGaO_3(ZnO)$ and $(InGaO_3)_2ZnO$, respectively.

When determining the phase relationships of the above-mentioned systems comprising FeO, the oxygen partial pressure $P(O_2)$ must be controlled. The phase equilibrium diagrams of these systems were determined in situ using thermogravimetric analysis, controlling the $P(O_2)$ in the gas phase. Among these systems, Y_2O_3–Fe_2O_3–FeO and Yb_2O_3–Fe_2O_3–FeO were particularly selected as case studies in Subsection 1.2.1.

The phase equilibrium diagram of the ternary system R_2O_3–A_2O_3–BO (R= a lanthanide element, In, or Sc; A = In, Fe, Ga, or Al; B = Mg, Mn, Co, Cu, or Zn) was determined from solid-phase reactions of R_2O_3, A_2O_3, and BO powders [8, 11]. These compounds were synthesized with the classical quenching method, in which the starting materials were sealed in platinum tubes and the mixtures rapidly cooled in water after heating for a predetermined time. The diagrams were constructed from the crystal structures of the synthesized powders, as identified by powder X-ray diffraction and electron beam diffraction methods. For example, the following compounds were discovered: $In_2O_3(ZnO)_m$ [23, 33–37], $InAlO_3(ZnO)_m$ [16], $InFeO_3(ZnO)_m$ [10, 14, 21], $(InFeO_3)_n(CuO)_m$ [9], $(InGaO_3)_n(CuO)_m$ [9], $InFeO_3(MnO)_m$ [38], and

$InGaO_3(MnO)_m$ [12], all of which are isostructural with $InGaO_3(ZnO)_m$ [8, 11, 15, 23, 39]. Among these, the $In_2O_3-Ga_2O_3-BO$ system (B = Zn, Mg, Cu, and Co) is discussed in Subsection 1.2.2.

As mentioned above, a series of phases is generally expressed by a composition formula with a certain variable (e.g., a natural number n). These phases are called "homologous[1] phases." For example, the series of vanadium oxide compounds VO_2, V_2O_3, V_3O_5, … is defined by the general formula V_nO_{2n-1}. Such phases are called Magnéli phases; meanwhile, phases with the general formula V_nO_{2n+1} are called Wadsley phases. Although Magnéli and Wadsley phases are given by different formulae, in the context of this book, these phases belong to the homologous phase. As described in Section 1.1, the compounds $InGaO_3(ZnO)$, $InGaO_3(ZnO)_2$, $InGaO_3(ZnO)_3$, … are generally referred to as homologous-phase $InGaO_3(ZnO)_m$; compounds belonging to homologous phases are termed "homologous compounds," and homologous compounds with the composition formula $InGaO_3(ZnO)$ are termed "homologous $InGaO_3(ZnO)$."

1.2.1 Phase Equilibrium Diagrams in the System $R_2O_3-Fe_2O_3-FeO$ (R = Y and Yb)

(RFeO$_3$) FeO (R = Y and Yb) and (RFeO$_3$)$_2$ FeO are isostructural with ($InGaO_3$)ZnO and ($InGaO_3$)$_2$ZnO, respectively. This subsection describes the Y_2O_3–Fe_2O_3–Fe and Yb_2O_3–Fe_2O_3–Fe systems, from which the homologous (RFeO$_3$)$_n$(BO) were synthesized. The phase equilibrium diagrams of these systems were determined in situ by thermogravimetric analysis under controlled oxygen partial pressure $P(O_2)$. Thermogravimetric analysis directly measures the weight change of a sample heated at a constant rate using a thermobalance. The total pressure is 1 atm, and the oxygen partial pressure is controlled by the mixing ratio of the CO_2 and H_2 gas. In analyzing the above systems, the temperature was set to 1200°C, and the oxygen partial pressure (measured using a stabilized zirconia electrolyte cell) was increased from 1.0 to 1.58×10^{-16} atm.

1.2.1.1 Y_2O_3–Fe_2O_3–FeO System at 1200°C

As mentioned above, the phase equilibrium diagram of the Y_2O_3–Fe_2O_3–Fe system was determined at 1200°C [19, 28]; we describe the subsystem Y_2O_3–Fe_2O_3–FeO. In this subsystem, Y_2O_3, Fe_2O_3 (hematite) and FeO (wüstite) have bixbyite, corundum, and rock salt structures, respectively. The binary Y_2O_3–Fe_2O_3 system includes $YFeO_3$ (distorted perovskite) and $Y_3Fe_5O_{12}$ (yttrium–iron garnet). The binary Fe_2O_3–FeO system has Fe_3O_4 (magnetite) with Fe^{2+} and Fe^{3+}. YFe_2O_4, a new phase composed of Y_2O_3–Fe_2O_3–FeO, lies between $YFeO_3$

[1] The term "homologous" has various meanings in different fields. For example, in biology, "homologous" means "corresponding in structure and in origin," as for example the wing of a bird and the foreleg of a horse [A: *Random House Dictionary*]. In organic chemistry, "homologous" refers to a series of organic compounds "having similar characteristics and structure but differing by a number of CH_2 groups" [B: *Collins English Dictionary*]. In crystal chemistry, the term is used for a series of compounds expressed by a general formula. For example, IGZO has a series of compounds group, e.g., $In_2Ga_2ZnO_7$, $InGaZn_2O_5$, $InGaZn_3O_6$, and so on. These compounds are called a "homologous" series.

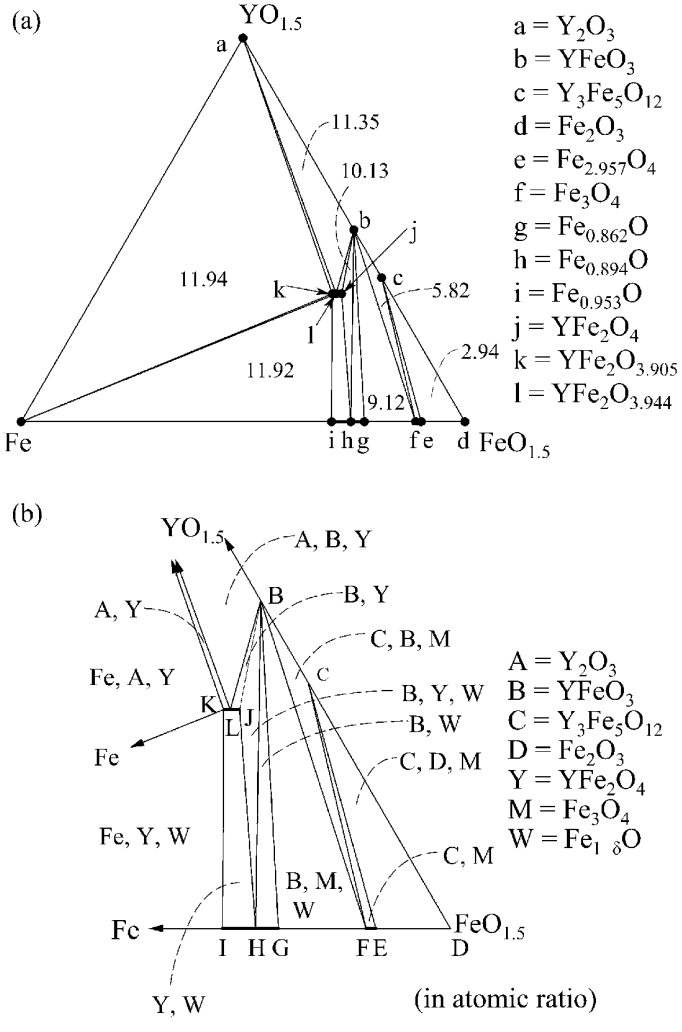

Figure 1.1 (a) Phase equilibrium diagram of the Y_2O_3–Fe_2O_3–Fe system at 1200°C and (b) detailed phase equilibrium diagram near $FeO_{1.5}$. ●, Single phase. In (a), the numbers signify the values of the $-\log P(O_2)$ fields equilibrated with the three solid phases. Small letters (a to l) in the diagram represent a chemical composition of a single phase as in the right of this figure. In (b), capital letters (A to M, W, and Y) in the diagram represent a phase of a chemical composition: letters A to L correspond to the small letters a to l in (a); letters M, W, and Y are as shown in the right of this figure. M is magnetite solid solution, W is partial solid solution of wüstite, and Y is solid solution or partial solid solution of YFe_2O_4. *Source*: Adapted from [28]

and FeO (shown in Figure 1.1) [28]. The YFe_2O_4 phase is isostructural with $InGaO_3(ZnO)$, as described later, and constitutes a mixed-valence compound with a layered structure of Fe^{2+} and Fe^{3+}. YFe_2O_4 was grown under controlled oxygen partial pressure by the floating zone method, and its crystal structure was determined by X-ray diffraction [19].

This YFe_2O_4 phase is stable at oxygen partial pressures $P(O_2)$ from 7.41×10^{-11} to 1.14×10^{-12} atm, and its chemical composition varies from $YFe_2O_{3.905}$ to $YFe_2O_{4.000}$. Above this $P(O_2)$ range, it decomposes into Y_2O_3 and metallic iron (γ-iron); below this range, it dissociates into $YFeO_3$ and wüstite (FeO). This dissociation is also observed at temperatures between 900 and 1100°C at a pressure of 4.9 GPa. A melt phase emerges at 1400°C. Under atmospheric pressure at 800°C, the YFe_2O_4 phase dissociates into an E phase (with a chemical composition of $Fe_{2.957}O_4$) and wüstite (FeO).

1.2.1.2 Yb_2O_3–Fe_2O_3–FeO System at 1200°C

Subsequent to the Y_2O_3–Fe_2O_3–Fe system, the next phase equilibrium diagram was constructed for the Yb_2O_3–Fe_2O_3–Fe system at 1200°C [29]; we describe the subsystem Yb_2O_3–Fe_2O_3–FeO. Homologous $(YbFeO_3)_nFeO$ (n = 1, 2, 3, and 4) were found as a new phase of this ternary system. Yb_2O_3 is a sesquioxide isostructural with the mineral bixbyite, similar to the above-mentioned Y_2O_3. However, the ionic radius of Yb^{3+} is smaller than that of Y^{3+} [40]. As with the Y_2O_3–Fe_2O_3–Fe system, the thermal equilibrium state of this system was analyzed at 1200°C under controlled partial oxygen pressure. In the $YbFeO_3$–FeO system, $YbFe_2O_4$ and $Yb_2Fe_3O_7$ are stable at oxygen partial pressures $P(O_2)$ ranging from 1.66×10^{-12} to 5.01×10^{-9} and 2.00×10^{-10} to 5.01×10^{-9} atm, respectively. Single crystals of $(YbFeO_3)$FeO and $(YbFeO_3)_2$FeO were grown, and their crystal structures were revealed [41]. Like the compounds in the Y_2O_3–Fe_2O_3–FeO system, the $YbFe_2O_4$ [18, 29] and $Yb_2Fe_3O_7$ [29, 42] in the Yb_2O_3–Fe_2O_3–FeO system are mixed-valence phases of Fe^{2+} and Fe^{3+}. These phases are isostructural with $InGaO_3(ZnO)$ and $(InGaO_3)_2ZnO$, respectively, as mentioned later. Figure 1.2 shows the phase equilibrium diagram of the Yb_2O_3–Fe_2O_3–FeO system at 1200°C. Note that $Yb_3Fe_4O_{10}$ and $Yb_4Fe_5O_{13}$ are generated as the heating temperature increases [43, 44].

1.2.2 Phase Equilibrium Diagram for the System In_2O_3–A_2O_3–BO (A = Ga and Fe; B = Zn, Mg, Cu, and Co)

In the phase equilibrium diagrams of the system R_2O_3–Fe_2O_3–FeO (R = Y and Yb), new phases were found; namely, YFe_2O_4 and $(YbFeO_3)_n$(FeO) (n = 1, 2, 3, and 4). Subsequently, the lanthanide element was replaced with an element of smaller ionic radius (indium), and the phase equilibrium diagram of the resulting system In_2O_3–A_2O_3–BO (where A is a trivalent cation and B is a divalent cation) was comprehensively investigated.

This subsection focuses on the relationship between the component BO (B = Zn, Mg, Cu, and Co) and the phase equilibrium diagram of the system In_2O_3–Ga_2O_3–BO. In these systems, each oxide has the following features: indium has a smaller ionic radius than a lanthanide; In_2O_3, like Y_2O_3 and Yb_2O_3, is isostructural with the mineral bixbyite. The indium cation in the oxide is trivalent with 4-, 5-, 6-, and 8-fold coordination [40]. In contrast, 4- and 5-fold coordination is unknown in rare-earth elements. The gallium oxide is isostructural with β-Ga_2O_3. The trivalent gallium cation has coordination numbers of four, five, and six. Empirically, trivalent gallium cations are known to favor four-coordinate cations more than trivalent iron cations. The divalent cations (B^{2+}) of Zn^{2+}, Co^{2+}, and Cu^{2+} are more inclined to be 4-fold coordinated

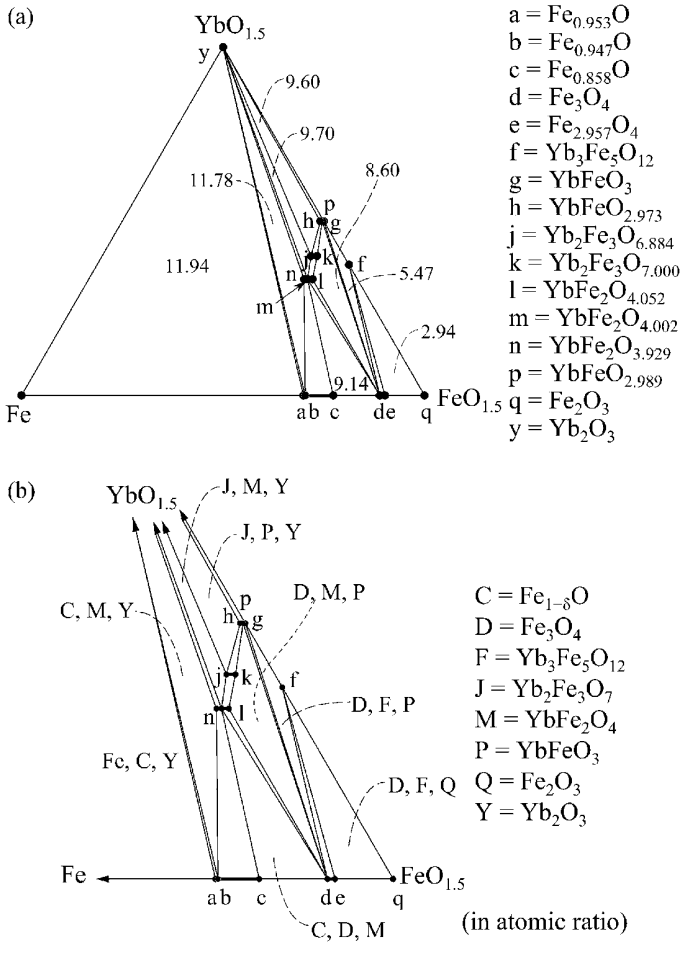

Figure 1.2 (a) Phase diagram of the system Yb_2O_3–Fe_2O_3–Fe at 1200°C and (b) detailed phase equilibrium diagram near $FeO_{1.5}$. ●, Experimental results. In (a), the numbers signify the values of the $-\log P(O_2)$ fields equilibrated with the three solid phases. Small letters (a to n, p, q, and y) in the diagram represent a chemical composition as in the right of this figure. In (b), capital letters in the diagram represent a phase corresponding to a chemical composition as in the right of this figure. These letters correspond to the small letters in (a). Solid solution of $YbFe_2O_4$ and $Yb_2Fe_3O_7$ exists in the range from l to n, and from j to k. $YbFe_2O_4$ and $Yb_2Fe_3O_7$ belong to homologous $(YbFeO_3)_n(FeO)$. *Source*: Adapted from [29]

than Fe^{2+}. The 4-fold coordination geometry of Co^{2+} and Cu^{2+} differs from that of Zn^{2+}, resulting in the difference in their crystallographic behavior.

In Subsections 1.2.2.1–1.2.2.4 we explain the phase equilibrium diagrams of two In_2O_3–Ga_2O_3–*B*O systems. In the first instance, *B* = Zn; in the second instance, *B* = Mg, Cu, and Co.

1.2.2.1 In_2O_3–Ga_2O_3–ZnO System at 1350°C

Under atmospheric pressure, the In_2O_3, Ga_2O_3, and ZnO in the In_2O_3–Ga_2O_3–ZnO system exhibit a bixbyite-type structure, a β-Ga_2O_3-type structure, and a wurtzite-type structure, respectively. At high temperature, Ga_2O_3 is a mineral corundum, as is Fe_2O_3. The In_2O_3–ZnO system contains hexagonal $In_2O_3(ZnO)_m$, whereas the Ga_2O_3–ZnO system contains orthorhombic $Ga_2O_3(ZnO)_m$. Likewise, the In_2O_3–Ga_2O_3–ZnO system contains $(InGaO_3)_2ZnO$ and $InGaO_3(ZnO)_m$. Figure 1.3 shows the phase diagram of the In_2O_3–Ga_2O_3–ZnO system. The regions (1)–(5) in this figure are explained below.

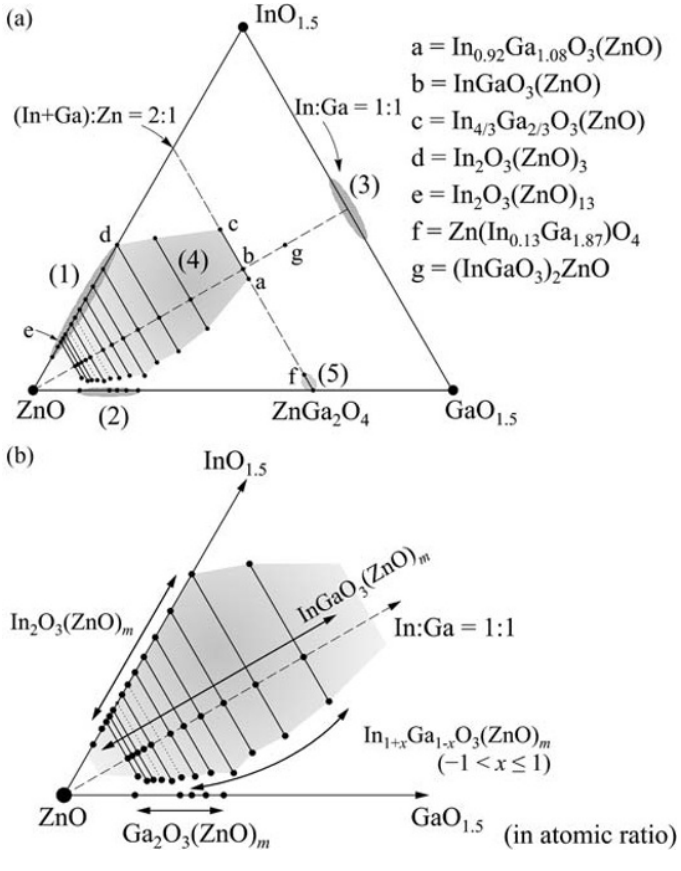

Figure 1.3 (a) Phase equilibrium diagram in the In_2O_3–Ga_2O_3–ZnO system at 1350°C and (b) detailed phase equilibrium diagram near ZnO. Filled circles (●) and solid lines connecting two filled circles are a single phase. (a) Small letters (a to g) in the diagram represent a chemical composition as in the right of this figure. Regarding homologous compounds, the solid lines connecting $In_2O_3(ZnO)_m$–$InGaO_3(ZnO)_m$–$In_{1+x}Ga_{1-x}O_3(ZnO)_m$ with the same m denote the solid-solution range. $InGaO_3(ZnO)_m$ and $InGaO_3(ZnO)_m$ have a hexagonal lattice, and $Ga_2O_3(ZnO)_m$ has an orthorhombic lattice. *Source*: Adapted from [15]

Region (1)

The In_2O_3–ZnO system contains $In_2O_3(ZnO)_m$ ($m \geq 3$). Kasper [33] reported on $In_2O_3(ZnO)_m$ ($m = 2, 3, 4, 5, 7$), Cannard and Tilley [34] reported on $In_2O_3(ZnO)_m$ ($m = 4, 5, 6, 7, 9, 11$), and Dupont *et al.* [35] reported on $In_2O_3(ZnO)_m$ ($m = 90$). $In_2O_3(ZnO)_m$ ($m = 5, 7$) does not decompose at temperatures above 1100°C; the other $In_2O_3(ZnO)_m$ single phases are stable at higher temperatures. For example, $In_2O_3(ZnO)_3$ is stable at 1265°C or higher, but decomposes into In_2O_3 and $In_2O_3(ZnO)_5$ at 1190°C, and into In_2O_3 and $In_2O_3(ZnO)_4$ at 1200°C [23].

Region (2)

The Ga_2O_3–ZnO system contains $ZnGa_2O_4$ (spinel type [45]) and $Ga_2O_3(ZnO)_m$ [46–49]. The crystal lattice of $Ga_2O_3(ZnO)_m$ is orthorhombic and differs from the hexagonal crystal lattice of $InGaO_3(ZnO)_m$. In the $Ga_2O_3(ZnO)_m$ crystal structure, all cations have 4-fold or 5-fold oxygen coordination; 6-fold coordination is not observed.

Region (3)

Under atmospheric pressure, the In_2O_3–Ga_2O_3 system has solid-solution phases of β-Ga_2O_3 and bixbyite In_2O_3; these phases co-exist at an In:Ga atomic ratio of 1:1. Hexagonal $InGaO_3$ is unstable under atmospheric pressure, but $InGaO_3$ isostructural with $YAlO_3$ forms under pressures higher than 0.3–1.5 GPa at 1100°C [50].

Region (4)

In the $InGaO_3$–ZnO system, $(InGaO_3)_2(ZnO)$ and $InGaO_3(ZnO)_m$ ($m \geq 1$) are present. $InGaO_3(ZnO)$ is isostructural with $YbFeO_3(FeO)$. An X-ray powder diffraction pattern confirms that $(InGaO_3)_2(ZnO)$ is isostructural with $(YbFeO_3)_2FeO$, although single crystals of this compound have yet to be synthesized. Layered structures in the $InGaO_3$–ZnO system can be approximately derived by stacking CdI_2-type and wurtzite-type structures, or by stacking $YAlO_3$-type and wurtzite-type structures. These crystal structures will be explained in Section 1.3. The In_2O_3–$ZnGa_2O_4$–ZnO system forms a solid solution of each $InGaO_3(ZnO)_m$ phase, and its solid solution ranges as $In_{1+x}Ga_{1-x}O_3(ZnO)_m$ ($m \geq 1$, $-1 < x \leq 1$, where x depends on m). When $m \geq 3$, the indium solid-solution limit of $In_{1+x}Ga_{1-x}O_3(ZnO)_m$ corresponds to $In_2O_3(ZnO)_m$ in the binary In_2O_3–ZnO system. In other words, solid solutions exist in the range $In_2O_3(ZnO)_m$ to $InGaO_3(ZnO)_m$ (Figure 1.3). Ga-rich compositions in the range $InGaO_3(ZnO)_m$ to $In_{1+x}Ga_{1-x}O_3(ZnO)_m$ ($m \geq 1$, $-1 < x < 0$) also form solid solutions [15, 39]. Layered Ga-rich structures form solid solutions over a narrow range; thus, no $Ga_2O_3(ZnO)_m$ is isostructural with $InGaO_3(ZnO)_m$. For example, in $(In + Ga) : Zn = 2 : 1$ (atomic ratio), $InGaO_3(ZnO)$ forms a solid solution in the range $In_{1.33}Ga_{0.67}O_3(ZnO)$ to $In_{0.92}Ga_{1.08}O_3(ZnO)$. Note that the system In_2O_3–A_2O_3–ZnO (A = Fe, Al) [14, 16] also contains $InAO_3(ZnO)_m$, which is isostructural with $InGaO_3(ZnO)_m$.

Region (5)

In $(In + Ga) : Zn = 2 : 1$ (atomic ratio), spinel-type $ZnGa_2O_4$ forms at the Ga-rich limit. The upper limit of the indium solid-solution range of $ZnGa_2O_4$ is approximately 3 mol% [15].

1.2.2.2 In_2O_3–Ga_2O_3–MgO System at 1300°C

In addition to the In_2O_3–Ga_2O_3–ZnO system, the In_2O_3–Ga_2O_3–*B*O system is likely to contain compounds isostructural with $(YbFeO_3)_nFeO$ and $InGaO_3(ZnO)_m$ and their solid solutions. The presence of such groups of compounds and their solid solutions depends on the combination of trivalent cations (In^{3+}, Ga^{3+}) and divalent cations. Here we describe the In_2O_3–Ga_2O_3–MgO system, which has a group of layered-structure compounds isostructural with the In_2O_3–Ga_2O_3–ZnO system, and whose spinel-type $MgGa_2O_4$ ($MgIn_2O_4$) has a wide range of substitutional solid solutions involving indium (gallium) cations.

The phase equilibrium diagram of the In_2O_3–Ga_2O_3–MgO system at 1300°C [13] allows layered-structure $InGaO_3(MgO)_m$ ($m = 1, 2$) and spinel-type $MgGa_2O_4$ (shown in Figure 1.4) [51, 52]. $InGaO_3(MgO)$ and $InGaO_3(MgO)_2$ are isostructural with $InGaO_3(ZnO)$ and $InGaO_3(ZnO)_2$, respectively. $InGaO_3(MgO)$ forms a solid solution in the composition range $InGaO_3(MgO)$ to $In_{1+x}Ga_{1-x}O_3(MgO)(x = 0.2)$ (solid line R–S in Figure 1.4). Like $InGaO_3(ZnO)$, $InGaO_3(MgO)$ retains its layered structure at various composition ratios of trivalent cations (In^{3+}, Ga^{3+}).

Unlike the In_2O_3–Ga_2O_3–ZnO system, the $MgIn_2O_4$–$MgGa_2O_4$ system has a wide range of spinel-type solid solutions. In the range $Mg(In_{2-x}Ga_x)O_4$ ($0 \le x \le 0.32$), Ga_2O_3 and $MgIn_2O_4$ are dissolved (solid line P–Q in Figure 1.4), whereas in the range $Mg(In_xGa_{2-x})O_4$ ($0 \le x \le 0.40$), In_2O_3 and $MgGa_2O_4$ mix (solid line U–V in Figure 1.4). In solid solutions of $MgIn_2O_4$ in which Ga substitutes for In, and of $MgGa_2O_4$ in which In substitutes for Ga, $Mg(In_{2-x}Ga_x)O_4$ and $Mg(In_xGa_{2-x})O_4$ have an inverse spinel-type structure.

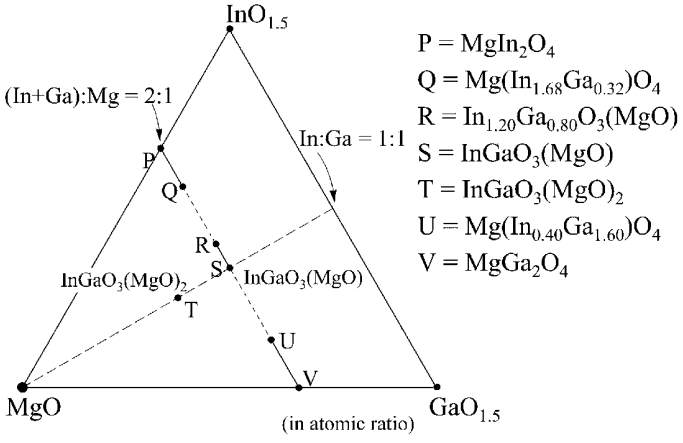

Figure 1.4 Phase equilibrium diagram in the In_2O_3–Ga_2O_3–MgO system at 1300°C. Filled circles (●) and solid lines connecting two filled circles are a single phase. Capital letters (P to V) in the diagram represent a chemical composition as in the right of this figure. At the triangle vertexes corresponding to $InO_{1.5}$, $GaO_{1.5}$, and MgO, the single phases In_2O_3, Ga_2O_3, and MgO exist, respectively. The line between P and V denotes $(In + Ga) : Mg = 2 : 1$. The dashed line extending from MgO denotes $In : Ga = 1 : 1$. The solid lines P–Q and U–V indicate a solid-solution range of the spinel-type structure, and the solid line R–S indicates a solid-solution range of the $YbFe_2O_4$-type structure. *Source*: Adapted from [13]

As mentioned above, the multi-component oxides of the In_2O_3–Ga_2O_3–MgO system have a narrow composition range for layered structures and a wide range for spinel-type structures. When $(In + Ga) : Mg = 2 : 1$, spinel-type structures form in the In-rich and Ga-rich limits, whereas layered structures form when In and Ga have approximately the same chemical composition.

1.2.2.3 In_2O_3–Ga_2O_3–CuO System at 1000°C

The In_2O_3–Ga_2O_3–CuO system substitutes Cu^{2+} for Zn^{2+} in the In_2O_3–Ga_2O_3–ZnO system. At 1000°C, this system includes bixbyite-type In_2O_3, β-Ga_2O_3-type Ga_2O_3, tenorite-type CuO, spinel-type $CuGa_2O_4$, and $Ho_2Cu_2O_5$-type $In_2Cu_2O_5$ [53]. The $InGaO_3$–CuO system includes $(InGaO_3)CuO$ and $(InGaO_3)_2CuO$, which are isostructural with $(YbFeO_3)FeO$ and $(YbFeO_3)_2FeO$, respectively. The homologous phases in the In_2O_3–Ga_2O_3–CuO system are shown in Figure 1.5, and their lattice constants are shown in Table 1.2. A phase isostructural

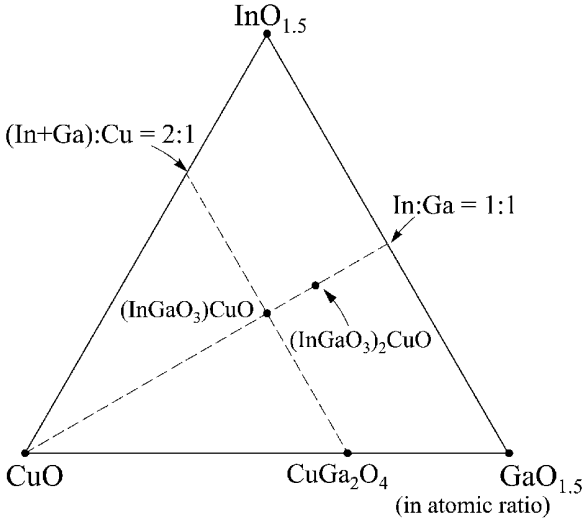

Figure 1.5 Phase equilibrium diagram in the In_2O_3–Ga_2O_3–CuO system at 1000°C. ● Indicates that $InGaO_3$(CuO) and $(InGaO_3)_2CuO$ are isostructural with $YbFeO_3$(FeO) and $(YbFeO_3)_2FeO$, respectively. *Source*: Adapted from [9]

Table 1.2 Lattice constants of homologous compounds in $(InGaO_3)_nCuO$ and $(InGaO_3)_nZnO$, both shown in a hexagonal system. *Source*: Adapted from [9, 15]

	$(InGaO_3)CuO$ [9]	$(InGaO_3)ZnO$ [15]
a [nm]	0.3350	0.3296
c [nm]	2.482	2.602
	$(InGaO_3)_2CuO$	$(InGaO_3)_2ZnO$
a [nm]	0.3332	0.3306
c [nm]	2.870	2.946

with $InGaO_3(ZnO)_m$ ($m \geq 2$) and its solid solution are not found, because the coordination geometry differs between Cu^{2+} and Zn^{2+}. CuO and ZnO have 4-fold oxygen coordination but exhibit different coordination geometry; square planar and tetrahedral, respectively. Therefore, the compounds in the In_2O_3–Ga_2O_3–CuO system are not isostructural with $InGaO_3(ZnO)_m$ ($m \geq 2$).

1.2.2.4 In_2O_3–Ga_2O_3–CoO System at 1300°C

At 1300°C, the In_2O_3–Ga_2O_3–CoO system includes bixbyite-type In_2O_3, β-Ga_2O_3-type Ga_2O_3, NaCl-type CoO, and spinel-type $CoGa_2O_4$. $InGaO_3(CoO)$ isostructural with $YbFe_2O_4$ also exists; however, there have been no reports on $(InGaO_3)_nCoO$ ($n \geq 2$), $InGaO_3(CoO)_m$ ($m \geq 2$), and a solid solution of $InGaO_3(CoO)$. The solid solution $Co(In_xGa_{2-x})O_4$ of indium-substituted $CoGa_2O_4$ is in the range $0.0 \leq x \leq 0.4$. The phase diagram of the In_2O_3–Ga_2O_3–CoO system (Figure 1.6) resembles that of In_2O_3–Ga_2O_3–MgO rather than In_2O_3–Ga_2O_3–ZnO, although the In_2O_3–CoO system contains no spinel-type $CoIn_2O_4$.

1.2.3 Phase Equilibrium Diagram of the System In_2O_3–A_2O_3–ZnO (A = Fe and Al)

The previous subsection described the phase diagram of the In_2O_3–Ga_2O_3–BO system (B = Zn, Mg, Cu, and Co), whose element combination determines the chemical composition ranges of

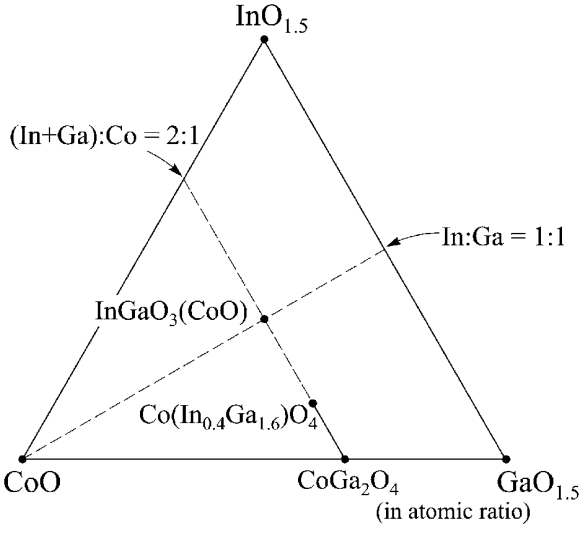

Figure 1.6 Phase equilibrium diagram in the In_2O_3–Ga_2O_3–CoO system at 1300°C. Plotted are $YbFe_2O_4$-type $InGaO_3(CoO)$ and spinel-type $CoGa_2O_4$. Indium solid solution of $CoGa_2O_4$ exists up to $In_{0.4}Ga_{1.6}O_3(CoO)$. The solid line shows the indium solid-solution range of $CoGa_2O_4$. *Source*: Adapted from [9]

the homologous compounds and the solid solutions. In fact, some $InGaBO_4$-type compounds are reported to contain compounds that take both layered and spinel-type structures; the In_2O_3–Ga_2O_3–MnO system contains spinel-type and $YbFe_2O_4$-type $InGaMnO_4$ [8].

Within the system In_2O_3–Ga_2O_3–BO (B = Zn, Mg, Cu, and Co), the In_2O_3–Ga_2O_3–ZnO system has the largest number of homologous phases, and $InGaO_3(ZnO)_m$ has a wide solid-solution range. This indicates that ZnO is currently the best combination for forming layered structures over a wide chemical-composition range in ternary oxide systems including In_2O_3 and Ga_2O_3.

The $In_2O_3-A_2O_3-ZnO$ (A = Ga, Fe, and Al) system forms layered structures over an extensive range of chemical compositions [14, 16]. The phase equilibrium diagram of the In_2O_3–Ga_2O_3–ZnO system was presented in Subsection 1.2.2.1; we now present the phase diagram of In_2O_3–A_2O_3–ZnO (A = Fe and Al).

1.2.3.1 In_2O_3–Fe_2O_3–ZnO System at 1350°C

Under atmospheric pressure, In_2O_3, Fe_2O_3, and ZnO in the In_2O_3–Fe_2O_3–ZnO system exhibit bixbyite-type, corundum-type, and wurtzite-type structures, respectively. The In_2O_3–ZnO system includes homologous compounds of the form $In_2O_3(ZnO)_m$. Likewise, the In_2O_3–Fe_2O_3–ZnO system includes homologous compounds of the form $InFeO_3(ZnO)_m$. The phase diagram of the In_2O_3–Fe_2O_3–ZnO system is shown in Figure 1.7. Regions (1)–(4) in that figure are explained below.

Region (1)

The In_2O_3–ZnO system contains $In_2O_3(ZnO)_m$ ($m \geq 3$) (see Subsection 1.2.2.1).

Region (2)

In addition to spinel-type $ZnFe_2O_4$, the Fe_2O_3–ZnO system includes $Fe_2O_3(ZnO)_m$ ($m = 12, 13$) [14], which is not isostructural with $InFeO_3(ZnO)_m$. $Fe_2O_3(ZnO)_m$ with smaller m exist at 1550°C [21].

Region (3)

In the $InFeO_3$–ZnO system, $InFeO_3(ZnO)_m$ ($m \geq 1$) is present. As with $InGaO_3(ZnO)$, $InFeO_3(ZnO)$ is isostructural with $YbFeO_3(FeO)$. In the In_2O_3–$ZnFe_2O_4$–ZnO system, each phase of $InFeO_3(ZnO)_m$ has a solid solution in the range $In_{1+x}Fe_{1-x}O_3(ZnO)_m$ ($m \geq 1$, $-1 < x \leq 1$, x depends on m). When $m \geq 3$, the limit of indium solid solution is $In_2O_3(ZnO)_m$. Solid solutions also form in Fe-rich compositions [14] over ranges that depend on m. Note that $In_{1+x}Fe_{1-x}O_3(ZnO)_m$ solid solutions exclude $Fe_2O_3(ZnO)_m$ in region (2), because this compound is not isostructural with $InFeO_3(ZnO)_m$.

Region (4)

The chemical composition $(In + Fe) : Zn = 2 : 1$ (atomic ratio) admits spinel-type $ZnFe_2O_4$. The indium solid solution of this compound ranges from $ZnFe_2O_4$ to $In_xFe_{2-x}O_3(ZnO)_4$.